

The role of LRG1 and LRG2's monopole in inferring the DESI 2024 BAO cosmology

Zhengyi Wang,^{1,2} Shijie Lin,^{1,2} Zhejie Ding,^{3,4} and Bin Hu^{1,2,*}

¹*Institute for Frontier in Astronomy and Astrophysics,
Beijing Normal University, Beijing 102206, China*

²*Department of Astronomy, Beijing Normal University, Beijing 100875, China*

³*Department of Astronomy, School of Physics and Astronomy,
Shanghai Jiao Tong University, Shanghai 200240, China*

⁴*Shanghai Key Laboratory for Particle Physics and Cosmology, Shanghai 200240, China*

The Dark Energy Spectroscopic Instrument (DESI) collaboration recently released its first year of data (DR1) on baryon acoustic oscillations (BAO) in galaxy, quasar, and Lyman- α forest tracers. When combined with CMB and SNIa data, DESI BAO results suggest potential thawing behavior in dark energy. Cosmological analyses utilize comoving distances along (D_H) and perpendicular to (D_M) the line of sight. Notably, there are $1 \sim 2\sigma$ deviations in D_M and D_H from Planck cosmology values in the luminous red galaxies (LRG) bins LRG1 and LRG2. This study examines the role of LRG1 and LRG2 in diverging DESI 2024 BAO cosmology from Planck cosmology. We use angle-averaged distance D_V and the ratio $F_{AP} = D_M/D_H$, which are more directly related to the measured monopole and quadrupole components of the galaxy power spectrum or correlation function, instead of the officially adopted D_M and D_H . This transformation aims to isolate the influence of monopoles in LRG1 and LRG2 on deviations from $w = -1$. Our findings indicate that removing the D_V data point in LRG2 aligns DESI + CMB + SNIa data compilation with $w = -1$ within a 2σ contour and reduces the H_0 discrepancy from the Planck 2018 results from 0.63σ to 0.31σ . Similarly, excluding the D_V data point from LRG1 shifts the w_0/w_a contour toward $w = -1$, although no intersection occurs. This highlights the preference of both LRG1 and LRG2 BAO monopole components for the thawing dark energy model, with LRG2 showing a stronger preference. We provide the D_V and F_{AP} data and their covariance alongside this paper.

I. INTRODUCTION

Dark energy was introduced to explain the discovery of the universe's accelerated expansion [1, 2]. Using measurements from standard rulers such as baryon acoustic oscillations (BAO), researchers can constrain whether dark energy behaves like a cosmological constant or exhibits physical dynamics. The equation of state of dark energy can be phenomenologically parameterized into the form of $w(z) = w_0 + w_a(1 - a)$ [3, 4], where a is the scale factor. The BAO signal was first detected by surveys such as the Sloan Digital Sky Survey (SDSS) [5] and the 2dF Galaxy Redshift Survey (2dFGRS) [6]. To achieve more precise distance determinations at the percent level, a new generation of galaxy clustering surveys, including the Six-degree Field Galaxy Survey (6dFGS) [7], the Baryon Oscillation Spectroscopic Survey (BOSS) [8], the extended Baryon Oscillation Spectroscopic Survey (eBOSS) [9], and the WiggleZ Survey [10], were conducted. These surveys have improved BAO distance determinations to an accuracy of $1 - 2\%$ at $z < 1$ [11–14], extended the BAO measurement at $z > 1$ [15–18], and found that dark energy was consistent with the cosmological constant [e.g. 19].

Recently, the Dark Energy Spectroscopic Instrument (DESI) survey [20–23], one of the Stage IV surveys [24–26], presented Data Release 1 (DR1) of BAO measurements from galaxy, quasar and Lyman- α forest tracers [27, 28] and the cosmological results derived from these measurements [29]. For the cosmological constraint, the DESI collaboration using the distance measurements (the comoving angular diameter distance, D_M and the comoving Hubble distance, D_H) alone and in combination with other cosmological probes such as the Big Bang Nucleosynthesis (BBN), the Cosmic Microwave Background (CMB), and Type Ia supernovae (SNIa), DESI provided cosmological inference results for various cosmological models, including the standard Λ CDM model, the w CDM model, and the w_0w_a CDM model. In particular, by fitting the w_0w_a CDM model to the DESI + CMB combination, the collaboration reported a significance of 2.6σ hint for the thawing dark energy model [30]. This significance persisted or increased when Pantheon+ [31], Union3 [32], or DES-SN5YR SNIa [33] were included, leading to results that were discrepant with the Λ CDM model at the levels of 2.5σ , 3.5σ , or 3.9σ , respectively.

The discrepancies with the Λ CDM model observed in DESI BAO data have prompted extensive discussions on dark energy. Several studies have sought to constrain various cosmological physics using the new DESI BAO data

* bhu@bnu.edu.cn

[34–44], while others have delved into the reasons behind the observed discrepancies [45–49]. We notice that the DESI distance D_H measurement in LRG1 ($z_{\text{eff}} = 0.510$) and D_M measurement in LRG2 ($z_{\text{eff}} = 0.706$) exhibit significant deviations from the fiducial Planck cosmology. Some studies have opted to reanalyze cosmological constraints without considering LRG1 [46–48]. For instance, Wang [48] shows that by combining DESI, Planck and Pantheon+ data, the LRG1 has little impact on the constraint on w_0, w_a parameter estimation. Similar conclusion was made by the DESI collaboration [29]. Comparing the Figure 12. and Figure 6. of Ref. [29], we can see that with or without DESI LRG1 does not change the conclusion. However, we should notice that the measurements of D_M and D_H in LRG1 and LRG2 exhibited a high level of correlation. The corresponding correlation coefficients of D_M and D_H are ~ -0.4 , as shown in Table 18 of Ref. [27].

The DESI BAO distance measurements are obtained by fitting ten-ish parameters to the galaxy clustering correlation function or power spectrum. The two most important fitting parameters are the isotropic BAO dilation α_{iso} and the anisotropic BAO dilation α_{AP} . We reference Table 5 in Ref. [27] for the detailed list of these fitting parameters. In the Fourier-space fitting framework, the galaxy power spectrum, $P(k, \mu)$, is written as a function of the wave number k and (cosine) angle μ . The coordinates (k, μ) in the true cosmology are related with those in the fiducial cosmology by

$$\begin{aligned} k_{\text{true}} &= \frac{\alpha_{\text{AP}}^{1/3}}{\alpha_{\text{iso}}} \left[1 + \mu_{\text{fid}}^2 \left(\frac{1}{\alpha_{\text{AP}}^2} - 1 \right) \right]^{1/2} k_{\text{fid}}, \\ \mu_{\text{true}} &= \frac{\mu_{\text{fid}}}{\alpha_{\text{AP}}} \left[1 + \mu_{\text{fid}}^2 \left(\frac{1}{\alpha_{\text{AP}}^2} - 1 \right) \right]^{-1/2}, \end{aligned} \quad (1)$$

where the subscript “true” and “fid” denote the quantities in the true and fiducial cosmologies, respectively. From Eq. (1), we can see that α_{iso} merely rescale the wave number but not the separation angle. It indicates that the constraining power on α_{iso} only comes from the monopole component of the galaxy power spectrum, namely the isotropic component. Meanwhile, α_{AP} enters simultaneously into the rescaling of the wave number and separation angle. Hence, it is involved both in the monopole and quadrupole components. Via a global fitting to the galaxy power spectrum or correlation function, one can get the posterior distribution of α_{iso} and α_{AP} . The final angle-averaged distance, $D_V(z)$, and Alcock-Paczynski (AP) factor, $F_{\text{AP}}(z)$, are given by

$$\frac{D_V(z)}{r_s} = \alpha_{\text{iso}} \frac{D_V^{\text{fid}}(z)}{r_s^{\text{fid}}}, \quad (2)$$

$$F_{\text{AP}}(z) = \frac{F_{\text{AP}}^{\text{fid}}(z)}{\alpha_{\text{AP}}}. \quad (3)$$

From these operations, one can see that the angle-averaged distance, $D_V(z)$, is constrained only by the monopole component of the galaxy power spectrum, but the AP factor, $F_{\text{AP}}(z)$, enters into both the monopole and quadrupole components. From Figure 7 of Ref. [27], one can see that the data quality of the monopole is much better than the quadrupole. Hence, instead of using the officially adopted D_M and D_H observables, we switch to D_V and F_{AP} variables for studying the influences of the monopole and quadrupole to the cosmological implications. Notably, the D_V data points in LRG1 and LRG2 deviate from the fiducial Planck cosmology at the level of $1 \sim 2\sigma$, as shown in Figure 15 of Ref. [27]. It motivates us to re-analyze the LRG1 and LRG2 by using D_V and F_{AP} instead. The rest of this paper are organised in the following ways. In Section II, we present the data and methodology. In Section III, we show our validation and the cosmological analysis without D_V or F_{AP} or both in LRG1 and LRG2, respectively. Finally, we briefly discuss our findings.

II. DATA AND METHOD

In this section, we first list the data compilation used for this study. In order to validate our result, we adopt the same CMB + BAO + SNIa compilation as the DESI BAO cosmology paper [29]. Then, we present the formulas for the data vector transformation from (D_M, D_H) to (D_V, F_{AP}) . The mean values and the covariance matrix of the new data vector are provided in this section.

- **CMB** We adopt the Planck 2018 data including the low- ℓ temperature (TT), polarization (EE) at multipoles $\ell < 30$, Planck (CamSpec) high- ℓ TTTEEE likelihood [50, 51], and Atacama Cosmology Telescope (ACT) DR6 CMB lensing likelihood [52] at multipoles $2 \leq \ell \leq 4000$.
- **BAO** We adopt the DESI DR1 BAO data derived from the bright galaxy sample (BGS), LRG, emission line galaxy (ELG), quasar and Lyman- α forest tracers.

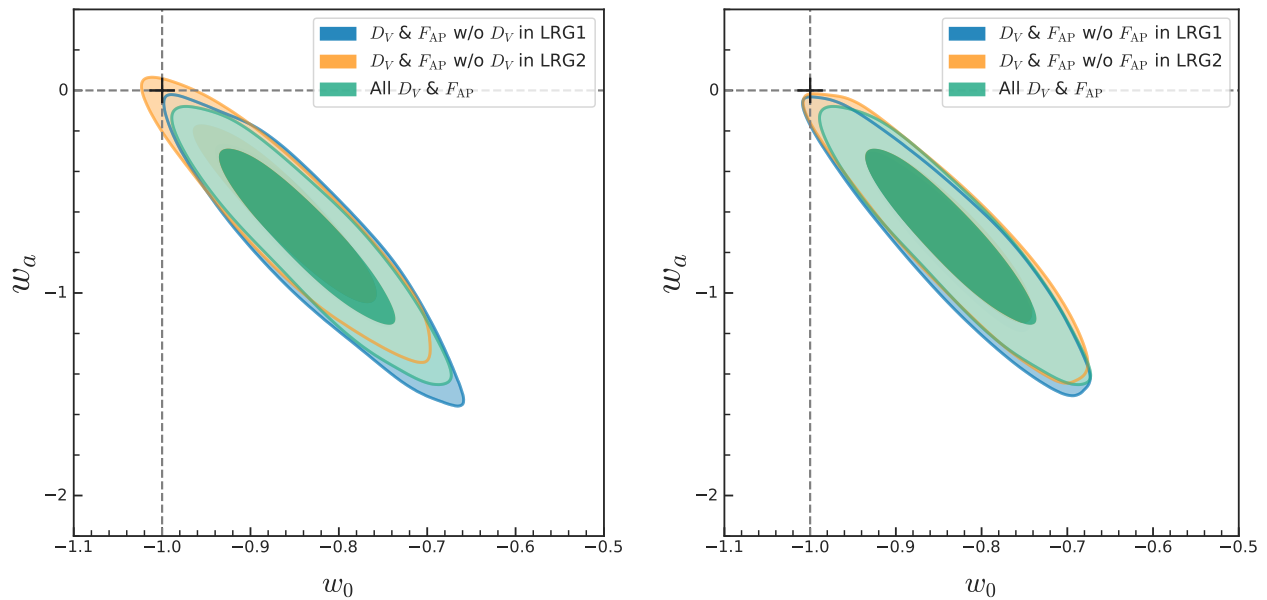


FIG. 1. **Left panel:** The marginalized posterior constraint on w_0 and w_a by removing D_V in LRG1 (blue), by removing D_V in LRG2 (orange) and by using all the D_V and F_{AP} data (green). **Right panel:** The marginalized posterior constraint on w_0 and w_a by removing F_{AP} in LRG1 (blue), by removing F_{AP} in LRG2 (orange) and by using all the D_V and F_{AP} data (green). The results of both panels are from DESI BAO combined with CMB and SNIa. The dark and light shaded region mark 1σ (68.3%) and 2σ (95.4%) confidence level (CL). The dashed lines and black cross mark the fiducial values of the two parameters in Λ CDM cosmology.

- **SN** We utilise the SNIa data from the Pantheon+ sample [31].

The sound horizon at the end of baryon drag epoch leaves an imprint in the distribution of matter, influencing the overdensity of galaxies, thus serving as a standard ruler [53, 54]. Measuring 2-point correlation function with position separation vector along the transverse direction, we can obtain the preferred angular separation $\Delta\theta = r_s/D_M$. Measuring position separation vector along the line-of-sight, we can obtain the preferred redshift separation $\Delta z = r_s H(z)/c = r_s/D_H$. We notice that D_M/r_s and D_H/r_s are highly correlated and have similar signal-to-noise ratio, hence, we adopt the spherically-averaged distance D_V to isolate isotropic and anisotropic signals. We follow the same definition of D_V and AP factor F_{AP} as in Ref. [55], *i.e.*

$$D_V = (zD_M^2 D_H)^{1/3}, F_{AP} = \frac{D_M}{D_H}. \quad (4)$$

For the brevity in the following equations, we define the following terms

$$d_M = \frac{D_M}{r_s}, d_H = \frac{D_H}{r_s}, d_V = \frac{D_V}{r_s} = (zd_M^2 d_H)^{1/3}, F_{AP} = \frac{d_M}{d_H}. \quad (5)$$

According to the propagation of uncertainties, we can calculate the covariance matrix of d_V and F_{AP} from the one of d_M and d_H by the following equation

$$\mathbb{C}_{\alpha\beta}(d_V, F_{AP}) = \mathcal{J}_{\alpha i} \mathbb{C}_{ij}(d_M, d_H) \mathcal{J}_{\beta j}^T, \quad (6)$$

where \mathbb{C} denotes the covariance matrix, and \mathcal{J} is the Jacobian matrix defined as

$$\mathcal{J} = \begin{bmatrix} \frac{\partial d_V}{\partial d_M} & \frac{\partial d_V}{\partial d_H} \\ \frac{\partial F_{AP}}{\partial d_M} & \frac{\partial F_{AP}}{\partial d_H} \end{bmatrix}. \quad (7)$$

Based on Table 1 of Ref. [29], we have the mean value and covariance matrices of D_M/r_s and D_H/r_s of different tracers. Therefore, we can obtain the mean value, standard deviation, and correlation coefficient of D_V/r_s and F_{AP} , via Eq. (6). We show the result in Table I.

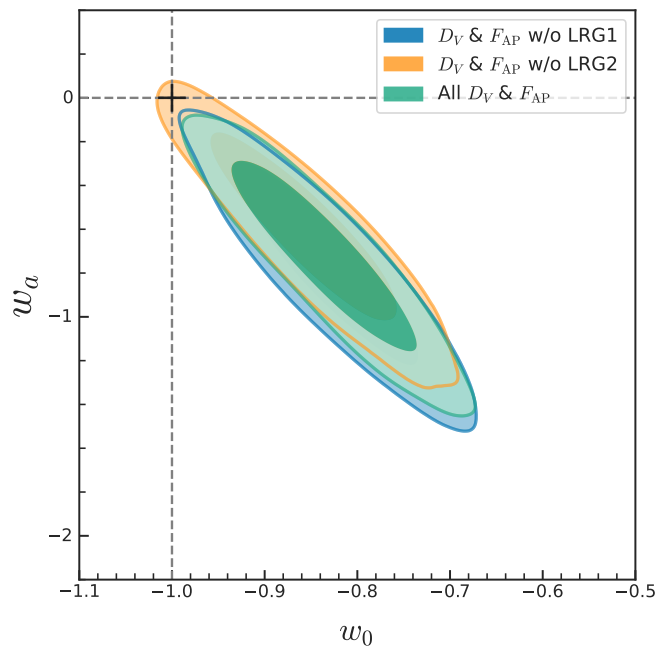


FIG. 2. The marginalized posterior constraint on w_0 and w_a by removing D_V and F_{AP} in LRG1 (blue), by removing D_V and F_{AP} in LRG2 (orange) and by using all the D_V and F_{AP} data (green). The dark and light shaded region mark 1σ (68.3%) and 2σ (95.4%) CL, respectively. The dashed lines and black cross mark the fiducial values of the two parameters in Λ CDM cosmology.

Tracer	z_{eff}	D_V/r_s	F_{AP}	r_{off}
BGS*	0.295	7.93 ± 0.151	-	-
LRG1	0.510	12.57 ± 0.149	0.65 ± 0.0265	0.0532
LRG2	0.706	15.90 ± 0.196	0.84 ± 0.0347	0.0495
LRG3+ELG1	0.930	19.86 ± 0.170	1.21 ± 0.0330	0.0864
ELG2	1.317	24.13 ± 0.365	2.01 ± 0.0948	0.2987
QSO*	1.491	26.07 ± 0.669	-	-
Ly α	2.330	31.52 ± 0.439	4.66 ± 0.1756	0.6052

TABLE I. The mean value and standard deviation of d_V and F_{AP} . $r_{\text{off}} = \sigma_{d_V, F_{AP}} / \sqrt{\sigma_{d_V} \sigma_{F_{AP}}}$ is the correlation coefficient between d_V and F_{AP} . The superscript ‘*’ denotes only d_V measured for the tracer.

We use the Boltzmann code `camb` [56] and the Bayesian analysis code `cobaya` [57, 58] to present the cosmological constraint results obtained from the Monte-Carlo Markov Chain (MCMC) method. In this study, we focus on the $w_0 w_a$ CDM cosmology. We analyze the MCMC chains using `getdist` [59]. We adopt the convergence diagnostic of the MCMC chains with the Gelman-Rubin [60] criterion $R - 1 \leq 0.01$. For each constraint, we execute 6 chains, each comprising $\sim 40,000$ steps, and remove 70% of the burn-in ($\sim 72,000$ samples remaining). We take the following uniform priors for model parameters: the baryon fraction $\Omega_b h^2 \in [0.005, 0.1]$, the cold dark matter fraction $\Omega_c h^2 \in [0.001, 0.99]$, assuming normal neutrino mass hierarchy $\sum m_\nu = 0.06 \text{eV}$, the Hubble parameter $H_0 \in [20, 100]$, the acoustic angular scale at the recombination epoch $100\theta_{\text{MC}} \in [0.5, 10]$, the amplitude of primordial power spectrum $\ln(10^{10} A_s) \in [2, 4]$, the primordial scalar spectral index $n_s \in [0.8, 1.2]$, and the reionization optical depth $\tau \in [0.01, 0.8]$.

Data	w_0	w_a
All D_V & F_{AP}	-0.834 ± 0.064	$-0.73^{+0.31}_{-0.27}$
w/o D_V in LRG1	$-0.835^{+0.060}_{-0.071}$	$-0.73^{+0.33}_{-0.26}$
w/o D_V in LRG2	-0.857 ± 0.067	-0.61 ± 0.29
w/o F_{AP} in LRG1	-0.834 ± 0.067	-0.76 ± 0.30
w/o F_{AP} in LRG2	-0.835 ± 0.066	-0.72 ± 0.29
w/o LRG1	-0.831 ± 0.065	$-0.77^{+0.31}_{-0.28}$
w/o LRG2	-0.853 ± 0.066	-0.61 ± 0.29

TABLE II. The marginalized posterior constraints on w_0 and w_a with 1σ (68.3%) C.L. are shown. In the “Data” column, “w/o D_V in LRG1” means that we employ D_V & F_{AP} of all tracers but exclude the data point of D_V in LRG1. Similarly, “w/o F_{AP} in LRG1” means that we employ D_V & F_{AP} of all tracers but not the F_{AP} in LRG1. “w/o LRG1” means that we employ all D_V & F_{AP} but exclude both D_V and F_{AP} in LRG1.

III. RESULTS

In the left panel of Figure 1, we show the constraints on w_0/w_a parameters by excluding the D_V data in either LRG1 (blue) or LRG2 (orange). The baseline setup, encompassing all D_V and F_{AP} data points, is depicted in green. It is apparent that excluding the D_V data points in LRG1 or LRG2 shifts the contours in the w_0/w_a plane towards the $w = -1$ point (identified by a bold black cross). The distinction lies in the fact that the “w/o LRG2” 2σ contour encompasses the $w = -1$ point, whereas the “w/o LRG1” contour does not. The right panel of Figure 1 shows the results by removing F_{AP} data in either LRG1 (blue) or LRG2 (orange). One can see that the overall trend is similar to the one for D_V , but with a smaller size of the shift. Regardless of whether the F_{AP} in LRG1 or LRG2 is excluded, the resulting 2σ contours do not intersect with the $w = -1$ point.

In Figure 2, we show the result of simultaneously removing D_V and F_{AP} in either LRG1 or LRG2. One can see that, the result of “w/o LRG2” is still consistent with $w = -1$ within 2σ confidence level; while the result of “w/o LRG1” are getting more closer to the one with “all” D_V and F_{AP} data points. This occurs because the D_V and F_{AP} in LRG1 pull the blue contour in slightly different directions (see Figure 1). By incorporating both these data points simultaneously, their effects cancel each other out, resulting in the contour remaining unchanged. This finding aligns the conclusion reported by Wang [48] and the DESI collaboration [29]. We summarise the marginalized posterior constraints on w_0 and w_a for various data compilations in Table II.

In Figure 3, we present the H_0 constraint results obtained by excluding various data points from DESI. If we remove a single D_V data point from either LRG1 or LRG2, the resulting H_0 estimate aligns more closely with the Planck result when the D_V data point is removed from LRG2 (orange) compared to LRG1 (blue). Additionally, if we also remove F_{AP} from the corresponding data bin, the H_0 estimate for LRG1 shifts even closer to the Planck result (red), while the estimate for LRG2 moves further away (green).

To safeguard the integrity of our findings against potential influences from factors such as inaccuracies in data vector transformation or convergence issues, we validate our results in both the (D_M, D_H) base and the (D_V, F_{AP}) base (refer to Figure 4 and Figure 5 in Appendix A). One can see that the two results perfectly align on top of each other.

For the first time, DESI BAO shows the hint of dynamical dark energy. This is an exciting result. In the meantime, we should remain cautious regarding the data. The BAO distance is derived from fitting the monopole and quadrupole components of galaxy clustering. Notably, we have observed unexpected discrepancies in both the monopole and quadrupole between the “true” cosmology and the fiducial cosmology in LRG1 and LRG2 datasets. This observation prompts us to investigate which observable serves as the primary driver behind this inconsistency. To achieve this objective, we convert the official (D_M, D_H) data vector to (D_V, F_{AP}) . This is because the latter is more directly linked to the monopole and quadrupole components in the galaxy clustering. Through a step-by-step exclusion of data points, we ascertain that the angle-averaged distance D_V in LRG2 predominantly favors the presence of dynamical dark energy. This suggests that we should allocate greater attention to the monopole component in LRG2 in the future DESI three-year and five-year analysis.

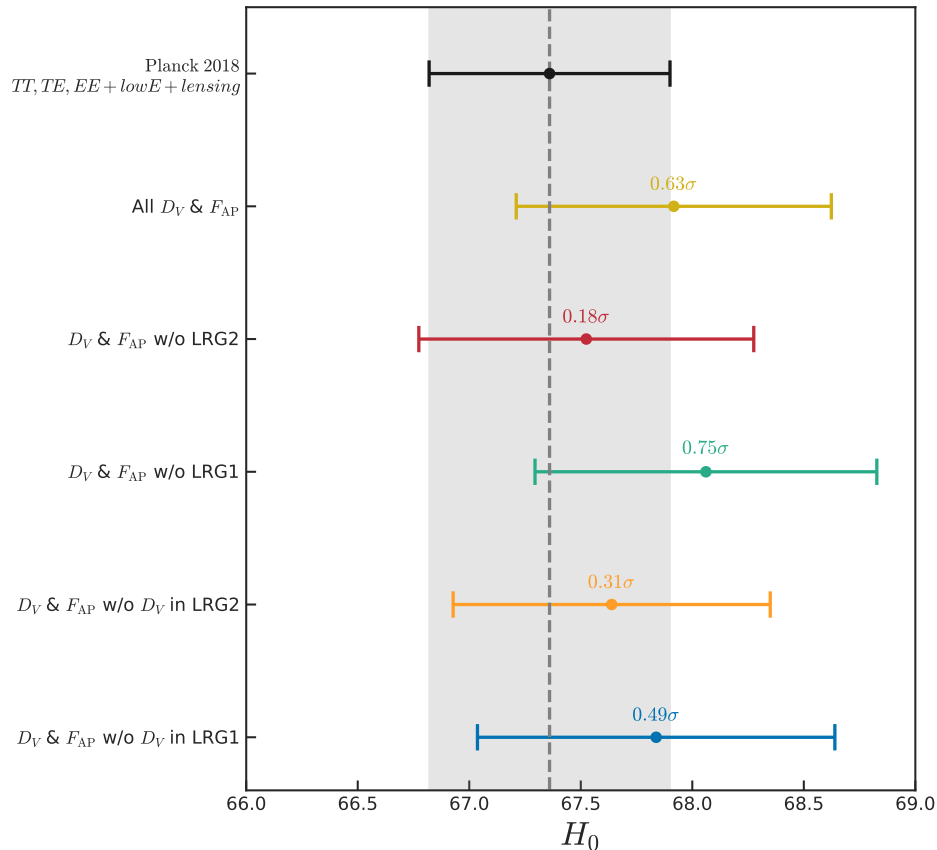


FIG. 3. The marginalized posterior constraint on H_0 from DESI and Planck. The colored numbers indicate the degree of tension between DESI and Planck, measured in units of standard deviation.

ACKNOWLEDGMENTS

ZW, SL and BH acknowledge the science research grants from the China Manned Space Project with No. CMS-CSST-2021-A12. ZD acknowledges the grant from the National Science Foundation with No. 12273020.

-
- [1] D. H. Weinberg, M. J. Mortonson, D. J. Eisenstein, C. Hirata, A. G. Riess, and E. Rozo, *Physics Reports* **530**, 87 (2013), arXiv:1201.2434 [astro-ph.CO].
 - [2] J. A. Frieman, M. S. Turner, and D. Huterer, *Annual Review of Astronomy and Astrophysics* **46**, 385 (2008), arXiv:0803.0982 [astro-ph].
 - [3] M. Chevallier and D. Polarski, *Int. J. Mod. Phys. D* **10**, 213 (2001), arXiv:gr-qc/0009008.
 - [4] E. V. Linder, *Phys. Rev. Lett.* **90**, 091301 (2003), arXiv:astro-ph/0208512.
 - [5] D. J. Eisenstein, I. Zehavi, D. W. Hogg, R. Scoccamarro, M. R. Blanton, *et al.*, *Astrophys. J.* **633**, 560 (2005), arXiv:astro-ph/0501171 [astro-ph].
 - [6] S. Cole, W. J. Percival, J. A. Peacock, P. Norberg, C. M. Baugh, *et al.*, *Monthly Notices of the Royal Astronomical Society* **362**, 505 (2005), arXiv:astro-ph/0501174 [astro-ph].
 - [7] F. Beutler, C. Blake, M. Colless, D. H. Jones, L. Staveley-Smith, L. Campbell, Q. Parker, W. Saunders, and F. Watson, *Monthly Notices of the Royal Astronomical Society* **416**, 3017 (2011), arXiv:1106.3366 [astro-ph.CO].
 - [8] S. Alam, M. Ata, S. Bailey, F. Beutler, D. Bizyaev, *et al.*, *Monthly Notices of the Royal Astronomical Society* **470**, 2617 (2017), arXiv:1607.03155 [astro-ph.CO].
 - [9] S. Alam, M. Aubert, S. Avila, C. Balland, J. E. Bautista, *et al.*, *Phys. Rev. D* **103**, 083533 (2021), arXiv:2007.08991 [astro-ph.CO].
 - [10] C. Blake, S. Brough, M. Colless, *et al.*, *Monthly Notices of the Royal Astronomical Society* **425**, 405 (2012), arXiv:1204.3674 [astro-ph.CO].

- [11] L. Anderson, É. Aubourg, S. Bailey, F. Beutler, V. Bhardwaj, *et al.*, Monthly Notices of the Royal Astronomical Society **441**, 24 (2014), arXiv:1312.4877 [astro-ph.CO].
- [12] F. Beutler, H.-J. Seo, A. J. Ross, P. McDonald, S. Saito, *et al.*, Monthly Notices of the Royal Astronomical Society **464**, 3409 (2017), arXiv:1607.03149 [astro-ph.CO].
- [13] Y. Wang, G.-B. Zhao, C.-H. Chuang, A. J. Ross, W. J. Percival, *et al.*, Monthly Notices of the Royal Astronomical Society **469**, 3762 (2017), arXiv:1607.03154 [astro-ph.CO].
- [14] J. E. Bautista, R. Paviot, M. Vargas Magaña, S. de la Torre, S. Fromenteau, *et al.*, Monthly Notices of the Royal Astronomical Society **500**, 736 (2021), arXiv:2007.08993 [astro-ph.CO].
- [15] J. E. Bautista, N. G. Busca, J. Guy, J. Rich, M. Blomqvist, *et al.*, Astronomy and Astrophysics **603**, A12 (2017), arXiv:1702.00176 [astro-ph.CO].
- [16] M. Ata, F. Baumgarten, J. Bautista, F. Beutler, D. Bizyaev, *et al.*, Monthly Notices of the Royal Astronomical Society **473**, 4773 (2018), arXiv:1705.06373 [astro-ph.CO].
- [17] J. Hou, A. G. Sánchez, A. J. Ross, A. Smith, *et al.*, Monthly Notices of the Royal Astronomical Society **500**, 1201 (2021), arXiv:2007.08998 [astro-ph.CO].
- [18] H. du Mas des Bourboux, J. Rich, A. Font-Ribera, V. de Sainte Agathe, J. Farr, *et al.*, Astrophys. J. **901**, 153 (2020), arXiv:2007.08995 [astro-ph.CO].
- [19] S. Alam *et al.* (eBOSS), Phys. Rev. D **103**, 083533 (2021), arXiv:2007.08991 [astro-ph.CO].
- [20] DESI Collaboration, A. Aghamousa, J. Aguilar, S. Ahlen, S. Alam, L. E. Allen, *et al.*, arXiv e-prints , arXiv:1611.00036 (2016), arXiv:1611.00036 [astro-ph.IM].
- [21] DESI Collaboration, B. Abareshi, J. Aguilar, S. Ahlen, S. Alam, D. M. Alexander, *et al.*, the Astronomical Journal **164**, 207 (2022), arXiv:2205.10939 [astro-ph.IM].
- [22] DESI Collaboration, A. G. Adame, J. Aguilar, S. Ahlen, S. Alam, G. Aldering, *et al.*, the Astronomical Journal **167**, 62 (2024), arXiv:2306.06307 [astro-ph.CO].
- [23] DESI Collaboration, A. G. Adame, J. Aguilar, S. Ahlen, S. Alam, G. Aldering, *et al.*, arXiv e-prints , arXiv:2306.06308 (2023), arXiv:2306.06308 [astro-ph.CO].
- [24] Euclid Science Collaboration, R. Laureijs, J. Amiaux, S. Arduini, J. L. Auguères, J. Brinchmann, *et al.*, arXiv e-prints , arXiv:1110.3193 (2011), arXiv:1110.3193 [astro-ph.CO].
- [25] D. Spergel, N. Gehrels, C. Baltay, D. Bennett, J. Breckinridge, *et al.*, arXiv e-prints , arXiv:1503.03757 (2015), arXiv:1503.03757 [astro-ph.IM].
- [26] LSST Science Collaboration, P. A. Abell, J. Allison, S. F. Anderson, J. R. Andrew, J. R. P. Angel, *et al.*, arXiv e-prints , arXiv:0912.0201 (2009), arXiv:0912.0201 [astro-ph.IM].
- [27] DESI Collaboration, A. G. Adame, J. Aguilar, S. Ahlen, S. Alam, D. M. Alexander, *et al.*, arXiv e-prints , arXiv:2404.03000 (2024), arXiv:2404.03000 [astro-ph.CO].
- [28] DESI Collaboration, A. G. Adame, J. Aguilar, S. Ahlen, S. Alam, D. M. Alexander, *et al.*, arXiv e-prints , arXiv:2404.03001 (2024), arXiv:2404.03001 [astro-ph.CO].
- [29] DESI Collaboration, A. G. Adame, J. Aguilar, S. Ahlen, S. Alam, D. M. Alexander, *et al.*, arXiv e-prints , arXiv:2404.03002 (2024), arXiv:2404.03002 [astro-ph.CO].
- [30] R. R. Caldwell and E. V. Linder, Phys. Rev. Lett. **95**, 141301 (2005), arXiv:astro-ph/0505494.
- [31] D. Scolnic, D. Brout, A. Carr, A. G. Riess, *et al.*, Astrophys. J. **938**, 113 (2022), arXiv:2112.03863 [astro-ph.CO].
- [32] D. Rubin, G. Aldering, M. Betoule, A. Fruchter, X. Huang, A. G. Kim, C. Lidman, E. Linder, S. Perlmutter, P. Ruiz-Lapente, and N. Suzuki, arXiv e-prints , arXiv:2311.12098 (2023), arXiv:2311.12098 [astro-ph.CO].
- [33] DES Collaboration, T. M. C. Abbott, M. Acevedo, M. Agüena, A. Alarcon, S. Allam, *et al.*, arXiv e-prints , arXiv:2401.02929 (2024), arXiv:2401.02929 [astro-ph.CO].
- [34] D. Wang, arXiv e-prints , arXiv:2404.06796 (2024), arXiv:2404.06796 [astro-ph.CO].
- [35] M. Cortès and A. R. Liddle, arXiv e-prints , arXiv:2404.08056 (2024), arXiv:2404.08056 [astro-ph.CO].
- [36] Y. Tada and T. Terada, (2024), arXiv:2404.05722 [astro-ph.CO].
- [37] O. Luongo and M. Muccino, arXiv e-prints , arXiv:2404.07070 (2024), arXiv:2404.07070 [astro-ph.CO].
- [38] K. V. Berghaus, J. A. Kable, and V. Miranda, arXiv e-prints , arXiv:2404.14341 (2024), arXiv:2404.14341 [astro-ph.CO].
- [39] W. Giarè, M. A. Sabogal, R. C. Nunes, and E. Di Valentino, arXiv e-prints , arXiv:2404.15232 (2024), arXiv:2404.15232 [astro-ph.CO].
- [40] I. J. Allali, A. Notari, and F. Rompineve, arXiv e-prints , arXiv:2404.15220 (2024), arXiv:2404.15220 [astro-ph.CO].
- [41] H. Wang and Y.-S. Piao, (2024), arXiv:2404.18579 [astro-ph.CO].
- [42] F. J. Qu, K. M. Surrao, B. Bolliet, J. C. Hill, B. D. Sherwin, and H. T. Jense, (2024), arXiv:2404.16805 [astro-ph.CO].
- [43] Y. Yang, X. Ren, Q. Wang, Z. Lu, D. Zhang, Y.-F. Cai, and E. N. Saridakis, (2024), arXiv:2404.19437 [astro-ph.CO].
- [44] C. Escamilla-Rivera and R. Sandoval-Orozco, (2024), arXiv:2405.00608 [astro-ph.CO].
- [45] W. Yin, (2024), arXiv:2404.06444 [hep-ph].
- [46] E. Ó. Colgáin, M. G. Dainotti, S. Capozziello, S. Pourojaghi, M. M. Sheikh-Jabbari, and D. Stojkovic, arXiv e-prints , arXiv:2404.08633 (2024), arXiv:2404.08633 [astro-ph.CO].
- [47] Y. Carloni, O. Luongo, and M. Muccino, arXiv e-prints , arXiv:2404.12068 (2024), arXiv:2404.12068 [astro-ph.CO].
- [48] D. Wang, arXiv e-prints , arXiv:2404.13833 (2024), arXiv:2404.13833 [astro-ph.CO].
- [49] C.-G. Park, J. de Cruz Perez, and B. Ratra, (2024), arXiv:2405.00502 [astro-ph.CO].
- [50] E. Rosenberg, S. Gratton, and G. Efstathiou, Monthly Notices of the Royal Astronomical Society **517**, 4620 (2022), <https://academic.oup.com/mnras/article-pdf/517/3/4620/46782205/stac2744.pdf>.

- [51] G. Efstathiou and S. Gratton, *The Open Journal of Astrophysics* **4** (2021), 10.21105/astro.1910.00483.
- [52] M. Madhavacheril, F. Qu, B. Sherwin, N. MacCrann, Y. Li, I. Abril-Cabezas, *et al.*, *The Astrophysical Journal* **962**, 113 (2024).
- [53] P. J. E. Peebles and J. T. Yu, *Astrophys. J.* **162**, 815 (1970).
- [54] R. A. Sunyaev and Y. B. Zeldovich, *Astrophysics and Space Science* **7**, 3 (1970).
- [55] DESI Collaboration, A. G. Adame, J. Aguilar, S. Ahlen, S. Alam, D. M. Alexander, *et al.*, arXiv e-prints, arXiv:2404.03002 (2024), arXiv:2404.03002 [astro-ph.CO].
- [56] A. Lewis, A. Challinor, and A. Lasenby, *Astrophys. J.* **538**, 473 (2000), arXiv:astro-ph/9911177 [astro-ph].
- [57] J. Torrado and A. Lewis, “Cobaya: Bayesian analysis in cosmology,” *Astrophysics Source Code Library*, record ascl:1910.019 (2019).
- [58] J. Torrado and A. Lewis, *J. Cosmol. Astropart. Phys.* **2021**, 057 (2021), arXiv:2005.05290 [astro-ph.IM].
- [59] A. Lewis, arXiv e-prints, arXiv:1910.13970 (2019), arXiv:1910.13970 [astro-ph.IM].
- [60] A. Gelman and D. B. Rubin, *Statistical Science* **7**, 457 (1992).

Appendix A: Validation

In order to examine the consistency of parameter constraints, particularly concerning the efficacy of (D_M, D_H) vs. (D_V, F_{AP}) in constraining w_0 and w_a , we present the consistency test from (D_M, D_H) versus (D_V, F_{AP}) with all tracers in Figure 4. We also check the agreement of the constraint from (D_M, D_H) versus (D_V, F_{AP}) with LRG1 or LRG2 excluded, as shown in Figure 5.

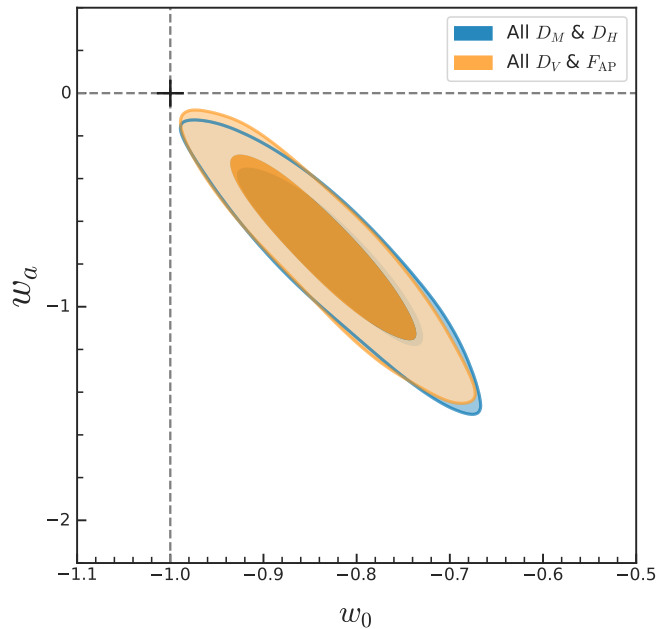


FIG. 4. The marginalized posterior constraint on w_0 and w_a comparison from all tracers of DESI BAO employing (D_M, D_H) (blue) and (D_V, F_{AP}) (orange). The dark and light shaded region mark 1σ (68.3%) and 2σ (95.4%) CL.

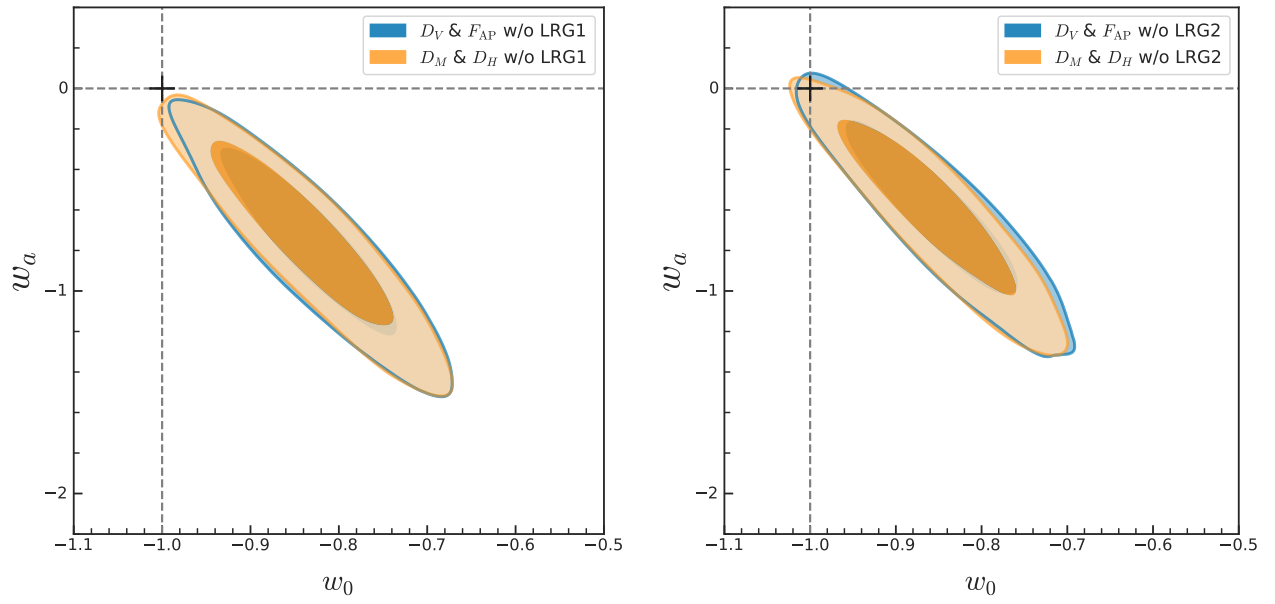


FIG. 5. **Left panel:** Comparison of the marginalized posterior constraint on w_0 and w_a from (D_V, F_{AP}) (blue) versus (D_M, D_H) (orange) with all tracers but not LRG1. **Right panel:** Comparison of the marginalized posterior constraint on w_0 and w_a from (D_V, F_{AP}) (blue) versus (D_M, D_H) (orange) with all tracers but not LRG2. The dark and light shaded region mark 1σ (68.3%) and 2σ (95.4%) CL.